Noname manuscript No.
(will be inserted by the editor)

Reconstructing Open Surfaces via Graph-Cuts

Min Wan, Yu Wang, Egil Bae, Xue-Cheng Tai, Desheng Wang

Received: date / Accepted: date

Abstract A novel graph-cuts-based method is proposed for reconstructing open surfaces from unordered point sets. Through a boolean operation on the crust around the data set, the open surface problem is translated to a watertight surface problem within a restricted region. Integrating the variational model, Delaunay-based tetrahedral mesh framework and multi-phase technique, the proposed method can reconstruct open surfaces robustly and effectively. Furthermore, a surface reconstruction method with domain decomposition is presented, which is based on the new open surface reconstruction method. This method can handle more general surfaces, such as non-orientable surfaces. The algorithm is designed in a parallel-friendly way and necessary measures are taken to eliminate cracks at the interface between the subdomains. Numerical examples are included to demonstrate the robustness and effectiveness of the proposed method on watertight, open orientable, open non-orientable surfaces and combinations of such.

Keywords Graph-cuts · Open Surface · Domain Decomposition · Delaunay triangulation

M. Wan, Y. Wang, X.-C. Tai, D. Wang
Division of Mathematical Sciences, School of Physical and Mathematical Sciences, Nanyang Technological University, Singapore 637371
E-mail: {wanm0003;wang0312}@e.ntu.edu.sg, {xctai;desheng}@ntu.edu.sg

E. Bae, X.-C. Tai
Department of Mathematics, University of Bergen, Johannes Brunsgate 12, 5007 Bergen, Norway
E-mail: {egil.bae;tai}@math.uib.no

1 Introduction

Reconstructing a surface from an unordered point data set has been a significant yet challenging problem in computer graphics for the last decade. Due to the development of three dimensional scanners and the increasing demand of computer graphics, extensive research has been conducted in the surface reconstruction field, much of which was dedicated to the watertight surface reconstruction for its topological simplicity and desirable properties. Open surface reconstruction problems, however, occur often in real applications, such as incomplete scanned data. As a topic which has been overlooked, the open surface reconstruction problem, to some extent, has more significance than the watertight surface problem for its topological generality.

Most surface reconstruction methods can be categorized into two groups, explicit methods and implicit methods. Explicit methods are mainly local geometric approaches based on Delaunay triangulation and dual Voronoi diagram such as Alpha shape and CRUST algorithm (Adamy et al, 2000; Amenta et al, 1998, 2000; Boissonnat and Cazals, 2000; Dey and Goswami, 2003; Edelsbrunner and Mucke, 1992). One advantage of these methods is their theoretical guarantee that there exists a sub-complex of Delaunay triangulation of the data set, which is homeomorphic to the ground truth surface given a sufficient sampling. Since these methods are local approaches, the global topological characteristics such as watertight or open, will not affect their performances. Their target is the potential homeomorphic sub-complex embedded in the Delaunay triangulation. The topology of the sub-complex surface does not make any difference. Hence, the explicit method can handle quite a number of open surface cases.

However, the explicit methods are subject to many reconstruction difficulties such as non-uniformity, undersampling and noises. Hence, during the last decade, variational models were brought into the reconstruction field. The reconstruction problem is formulated as a minimization problem of an energy functional defined over surfaces. To minimize an energy functional with respect to the surface, a consistent parametrization of the surface is not always available during the optimization procedure. As a result, researchers turned to the implicit methods (Alexa et al, 2001; Curless and Levoy, 1996; Franchini et al, 2010a,b; Hoppe et al, 1992; Ohtake et al, 2005; Solem and Heyden, 2004; Solem and Kahl, 2004, 2005; Solem and Overgaard, 2005; Ye et al, 2010; Zhao et al, 2001), such as the level set method, to gain flexibility of representation and mathematical facilities. One important such level set approach to the surface reconstruction problem was proposed by Zhao in (Zhao et al, 2001; Zhao, 2000). Graph cut is another tool that can minimize energy functions over implicitly defined surfaces. It has been applied to the surface reconstruction problem in (Hornung and Kobbelt, 2006b; Lempitsky and Boykov, 2007; Paris et al, 2006). The main advantages of graph cuts are the efficiency and ability to find global minima. However, the competence of both the level set method and graph cuts is lost on more general topologies (Osher and Fedkiw, 2002). One way to handle open surface problems with implicit methods is the use of multiple level set functions (Bertalmío et al, 1999; Burchard et al, 2001; Cheng et al, 2002; Faugeras and Gomes, 2000; Smereka, 2000; Solem and Heyden, 2006). Some hierarchical approaches have been experimented on some open surface problems (Hornung and Kobbelt, 2006b). However, these methods for open surfaces lack generality and robustness. In this article, a novel variational reconstruction method for open surfaces is proposed. The variational model, level set function, Delaunay triangulation and graph-cuts are integrated into a method competent of handling not only open surfaces but also general surfaces.

In the proposed method, the data set points as well as the properly generated background points are inserted to an unstructured tetrahedral mesh framework in a Delaunay way. Due to its nearest connection property, the Delaunay triangulation combining a sufficient sampling density provides a theoretic guarantee that there exists a sub-complex of the Delaunay triangulation such that it is homeomorphic to the ground truth surface. In the tetrahedral mesh, a crust is established around the data set. In (Wan et al, to appear), a graph dual to the whole mesh is built according to the energy functional and applied with max-flow/min-cut algorithms. Since these algorithms finds a global minimum, it is essential to specify boundary conditions of the crust. This can only be accomplished under the assumption that the domain can be separated into two or more subdomains by the watertight crust, which does not hold any more for an open surface problem. Without specifying boundary conditions, the dual graph does not have valid n-links to both source and sink, resulting in the minimal cut being trivial.

To tackle this issue, a boolean operation is proposed to restrict the region of interest within a narrow band, which can be separated into two or more subdomains. In the proposed method, two crusts with different thickness are built around the data set. The medial axis of the thick crust is to be obtained. One more crust is then built around the boundary of the medial axis. Subsequently, the two crusts around the data set are trimmed by the crust around the boundary. The trimmed thick crust can be separated by the trimmed thin crust. Hence in the restricted region, i.e. the trimmed thick crust, the trimmed thin crust is watertight such that region growing algorithms and graph cut techniques can be applied. More details and illustrations of this series of operations are provided in Section 3. The method subsequently constructs a graph dual to the restricted mesh, applies max-flow/min-cut algorithms and extracts the surface from the tetrahedral mesh according to the obtained minimal cut. These stages are the same as those in the watertight surface reconstruction method described in Section 2.

Furthermore, a surface reconstruction method based on domain decomposition is presented. The domain decomposition idea has been applied to computer vision (Kohlberger et al, 2003, 2004, 2005). Recently it is found also useful as a robust alternating minimization scheme between overlapped subspaces (Tai and Duan, 2009; Tai and Xu, 2002). In the decomposition method, the whole domain is decomposed into several subdomains. In each subdomain, a surface reconstruction problem, input of which is a subset of the whole data points, is solved. Merging all the surface patches from different subdomains is the critical task. Such a fix-the-boundary measure is taken before the graph technique is applied that potential conflicts and cracks can be eliminated effectively. The parallel efficiency may be undermined due to the interaction between subdomains. However, it can be compensated largely by a proper decomposition scheme. The method proposed in this article can handle not only open surfaces but also more general surfaces such as combinations of open and watertight surfaces.

The remainder of this paper is organized as follows. In Section 2, a brief review of watertight surface reconstruction based on delaunay triangulation and graph-

cuts will be given. Section 3 deals with the open surface problem. The new method to tackle this problem is proposed and the algorithm is given in details. Section 4 gives an important application of the open surface reconstruction method, the surface reconstruction based on domain decomposition, which can handle more general surfaces. To the best of our knowledge, this is the first attempt to approach the nonorientable surface reconstruction problem via graph-cuts. In Section 5 various numerical examples are presented to demonstrate effectiveness and robustness of the proposed method on all kinds of surfaces. Finally, Section 6 concludes the article.

2 Graph-cuts Reconstruction of watertight surface

In the previous work (Wan et al, to appear) a variational reconstruction method was proposed for watertight surfaces based on graph-cuts. The cost energy functional is a generalization from that of the weighted minimal surface model (Zhao et al, 2001), which is also related to the minimal surface (Caselles et al, 1997b) or geodesic active contours (Caselles et al, 1997a) approaches. This functional is minimized on an unstructured tetrahedral mesh framework, which provides more flexibility and effectiveness than structured grids used in other graph-based methods (Hornung and Kobbelt, 2006a,b; Paris et al, 2006). As a matter of fact, the Delaunay-based mesh guarantees the existence of a subcomplex homeomorphic to the ground truth surface given a sufficient sampling. The method can handle various reconstruction difficulties such as noise, undersampling and non-uniformity. By adopting the idea presented in (Bae and Tai, 2009), the method is able to address two phase and multi-phase problems in a unified approach. In addition, an automatic phase detecting method based on region growing algorithms is developed to minimizes user intervention. Since the ideas and techniques developed in (Wan et al, to appear) are the building blocks of this paper, a brief review will be given in this section.

2.1 Two phase surface reconstruction via graph-cuts

For convenience, this subsection only discusses two phase problems, in which the ground truth surface S simply separates the embedding domain $X \subset R^3$ into two connected regions, inside and outside. Let P be a point data set sampled from S in the domain X. Define the distance function as $d(x) = d(x, P) = \inf_{y \in P} d(x, y)$, where $d(x, y)$ is the Euclidean distance between points x and y in R^3. As in (Wan et al, to appear; Zhao et al, 2001), the following cost energy is proposed for surface reconstruction,

$$E(\Gamma) = \int_X |\phi_\Gamma(x) - I(x)|\, \beta(x) dx + \int_\Gamma d(x) ds + \alpha \int_\Gamma ds\,. \quad (1)$$

The above $\phi_\Gamma(x)$ is the piecewise constant level set function same as (Lie et al, 2006) corresponding to the surface Γ

$$\phi_\Gamma(x) = \begin{cases} c_1 \text{ if } x \text{ inside } \Gamma \\ c_2 \text{ if } x \text{ outside } \Gamma \end{cases}. \quad (2)$$

As a consequence, the surface Γ is implicitly represented as the discontinuities of $\phi_\Gamma(x)$.

The crust around P is defined as $C_d^P = \{x \in X : d(x, P) \leq d\}$. Given a watertight surface and a reasonably dense sampling, we assume the crust around the sampling data set is able to partition the whole domain into two connected regions, i.e. interior and exterior. $I(x)$ is an indicator function which labels these two subdomains as well as the crust region. Compared with $\phi_\Gamma(x)$ which labels the final partitioning , this indicator function serves as an initial labelling.

$$I(x) = \begin{cases} 0 \text{ if } x \text{ in } C_d^P \\ c_1 \text{ if } x \text{ in the interior part of } X \backslash C_d^P \\ c_2 \text{ if } x \text{ in the exterior part of } X \backslash C_d^P \end{cases}. \quad (3)$$

In (1), $\beta(x)$ is a confidence function suggesting the extent to which the indicator function, the estimate for the level set function, is faithful. The reconstructed surface is rather unlikely to fall outside the crust region given a low noise level, which results in the following specification of $\beta(x)$.

$$\beta(x) = \begin{cases} 0 \text{ if } x \text{ in } C_d^P \\ \sigma \text{ others} \end{cases}, \quad (4)$$

where σ is a relatively large positive value.

The first term in (1), can be viewed as specifying boundary conditions on ϕ at the boundary of the crust. By specifying proper $I(x)$ and $\beta(x)$, the first term would constrain the resulting surface within a restricted region, i.e. C_d^P. Otherwise, if there is any disagreement between $\phi_\Gamma(x)$ and $I(x)$ out of the crust region where $\beta(x) = \sigma$, the energy would not be minimized. This term is important, otherwise the global minimum of (1) would be the trivial null surface, where ϕ_Γ is just a constant everywhere. The second term is the essential part in the weighted minimal surface model (Zhao et al, 2001) and the third term is the regularization term concerning the surface area. By tuning the regularization coefficient α, a compromise between faithfulness and smoothness can be achieved.

In this method, (1) is discretized on an unstructured tetrahedral mesh $\mathcal{T}_h$ instead of structured grids used in

other graph-based methods. In this article, a mesh and triangulation are referring to the same thing (George and Borouchaki, 1998). Generally, a mesh can be defined by a pair (V, C). V is the set of all vertices and C is a complex consisting of four types of simplexes, i.e. vertices, edges, triangles, and tetrahedra. For vertices u, v, w, z, we define $\{v, u\}$ as the edge between v and u, $\{v, u, w\}$ as the triangle with vertices v, u, w, and $\{v, u, w, z\}$ as the tetrahedron with vertices v, u, w, z. $\{K_i\}_{i=1}^N$ are used to denote all N tetrahedra in $\mathcal{T}_h$. In our case V is the set of mesh points including data points and background points $P \cup Q$.

In a mesh $\mathcal{T}_h$, we can define 1-ring neighborhood of a vertex v as $N_v^1 = \{u | \{v, u\} \in C\}$ and M-ring neighborhood in a recursive way $N_v^M = \{u | \exists w \in N_v^{M-1}, \{w, u\} \in C\}$. Based on this neighborhood system, the crust around the data set P can be defined as $K_M^P = \{K_i | \exists v \in K_i, v \in N_u^M, u \in P\}$.

In this mesh framework, the surface Γ can be approximated by Γ_h, a sub-complex of $\mathcal{T}_h$. (Amenta et al, 1998) shows that there exists a sub-complex of the Delaunay triangulation of P, which is homeomorphic to the ground truth surface S. As a consequence of this fact and the local property of Delaunay triangulations, there also exists a homeomorphic-to-S sub-complex of the Delaunay triangulation of $Q \cup P$ given a reasonable distribution of background points Q.

The first term, the integral over the whole domain X can be simply discretized as

$$\begin{aligned} &\int_X |\phi_\Gamma(x) - I(x)| \, \beta(x) dx \\ &= \sum_{i=1}^N \int_{K_i} |\phi_\Gamma(x) - I(x)| \, \beta(x) dx \\ &\approx \sum_{i=1}^N |\phi_{\Gamma_h}(K_i) - I(K_i)| \, \beta(K_i) \, . \end{aligned} \tag{5}$$

$$\phi_{\Gamma_h}(K_i) = \begin{cases} c_1 \text{ if } K_i \text{ inside } \Gamma_h \\ c_2 \text{ if } K_i \text{ outside } \Gamma_h \end{cases} , \tag{6}$$

$$I(K_i) = \begin{cases} 0 \text{ if } K_i \in K_M^P \\ c_1 \text{ if } K_i \text{ in the interior} \\ c_2 \text{ if } K_i \text{ in the exterior} \end{cases} , \tag{7}$$

$$\beta(K_i) = \begin{cases} 0 \text{ if } K_i \in K_M^P \\ \sigma \text{ others} \end{cases} , \tag{8}$$

where σ is a relatively large positive value.

The second and third terms in (1) are integrals over the surface area. The surface triangulation Γ_h can be thought of as the union of the triangular faces shared by tetrahedra with different level set values.

$$\Gamma_h = \bigcup_{\phi_\Gamma(K_i) \neq \phi_\Gamma(K_j)} \Gamma_{ij} \, ,$$

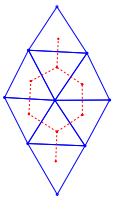

Fig. 1 The primal-dual relationship of triangular mesh.

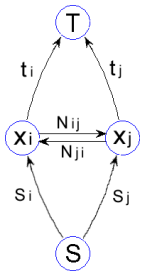

Fig. 2 Illustration of the assignment of graph edge weights.

where $\Gamma_{ij} = K_i \cap K_j$. Hence combining the result of (5), (1) can be discretized as follows

$$\begin{aligned} E(\Gamma) \approx &\sum_{i=1}^N |\phi_{\Gamma_h}(K_i) - I(K_i)| \, \beta(K_i) \\ &+ \sum_{i,j} (d_{ij} + \alpha) S_{ij} \mathbf{1}_{\{\phi_{\Gamma_h}(K_i) \neq \phi_{\Gamma_h}(K_j)\}} \, , \end{aligned} \tag{9}$$

where

$$d_{ij} = \frac{\int_{\Gamma_{ij}} d(x) ds}{\int_{\Gamma_{ij}} ds} \quad , \quad S_{ij} = \int_{\Gamma_{ij}} ds \, . \tag{10}$$

The energy of $E(\Gamma)$ can be minimized very efficiently by graph-cuts, since this energy functional is graph representable, which can be verified by the conclusion of (Kolmogorov and Zabin, 2004). Graph-cuts was also used in (Wan et al, to appear) to approach the energy optimization for watertight surfaces with connected interior and exterior. Therefore, a graph dual to the primal tetrahedral mesh is constructed, in which each node corresponds to a tetrahedron in the mesh and each edge corresponds to a triangular face in mesh. This primal-dual relationship is illustrated for two dimensions in Fig 1.

The edge weights are determined by different terms in $E(\Gamma)$ as shown in Fig 2 and below

$$\begin{aligned} s_i = |I(K_i) - c_2| \, \beta(K_i) \, , \; t_i = |I(K_i) - c_1| \, \beta(K_i) \, , \\ N_{ij} = (d_{ij} + \alpha) S_{ij} \, , \qquad N_{ji} = (d_{ij} + \alpha) S_{ij} \, , \end{aligned} \tag{11}$$

where c_1 and c_2 are the piecewise constant level set function values, standing for the regions inside and outside the surface.

Table 1 Relationship between cut and surface

Cut in dual graph	Surface in primal mesh
$C = \bigcup_{x_i,x_j \in V,\ \phi_i \neq \phi_j} (x_i, x_j)$	$\Gamma = \bigcup_{K_i,K_j \in \mathcal{T}_h,\ \phi_i \neq \phi_j} (K_i \cap K_j)$

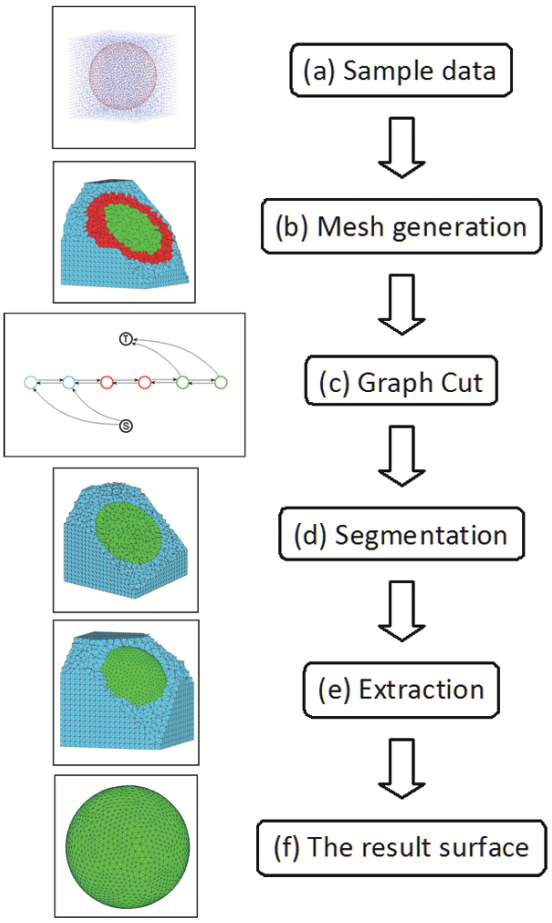

Fig. 3 Watertight surface reconstruction. Given a data set (a) sampled from an object surface, proper background points such as grid points are generated according to the data points distribution. An unstructured tetrahedral mesh (b) is generated in a Delaunay way and the crust around the data set is established. A graph dual to the mesh is constructed (c). Graph-cuts are applied and segmentation on the primal mesh is obtained (d). Extract the surface from tetrahedral mesh (e), the reconstructed surface is obtained (f).

After graph construction, max-flow/min-cut algorithms can be applied on the obtained graph. The algorithm in (Boykov and Kolmogorov, 2004) is a good choice for its empirically good performance. Due to the primal-dual relationship and its consequence about surface and cut as Table 1, the reconstructed surface can be directly extracted from the background mesh according to the minimal cut. The whole algorithm is shown in Table 2 and the flow chart is shown in Fig 3.

Table 2 Watertight surface reconstruction method

Inputs	A data point set P
Algorithm	
1.	Generate background points Q according to the density of P
2.	Insert P and Q to a tetrahedral mesh $\mathcal{T}_h$ in a Delaunay way
3.	Establish the crust, K_P^M
4.	Region growing on the regions outside K_P^M
5.	Specify the Indicator function according to (3)
6.	Construct a graph dual to the mesh
7.	Assign edge weights according to (11)
8.	Apply the graph-cuts
9.	Extract the surface according to the minimal cut
Outputs	The surface triangulation S

2.2 Multi-phase surface reconstruction

We assume now that the interior and exterior of the surface are not connected sets. Such cases can be handled by introducing more labels. We assume the surface separates X into M connected regions $\{X_i\}_{i=1}^M$. Surfaces of this kind can be represented in the level set framework of (Lie et al, 2006) by defining ϕ_Γ as $\phi_\Gamma(x) = c_i$ for $x \in X_i$, $i = 1, ..., M$. As before, Γ is represented as the discontinuities of ϕ_Γ. The complete energy functional (1) is therefore given in the discrete setting as

$$E(\Gamma) \approx \sum_{i=1}^{N} |\phi_{\Gamma_h}(K_i) - I(K_i)|\, \beta(K_i) + \sum_{i,j} (d_{ij} + \alpha) S_{ij} \mathbf{1}_{\{\phi_{\Gamma_h}(K_i) \neq \phi_{\Gamma_h}(K_j)\}} \tag{12}$$

where

$$d_{ij} = \frac{\int_{\Gamma_{ij}} d(x) ds}{\int_{\Gamma_{ij}} ds} \quad , \quad S_{ij} = \int_{\Gamma_{ij}} ds\,. \tag{13}$$

Minimization problems with multiple phases, or labels, have been studied previously in image processing. The work of (Ishikawa, 2003) and a later modification (Bae and Tai, 2009) presented techniques to efficiently minimize certain such multilabel problems by graph cuts. By making a simplification of the length term in (12), we can convert the problem (12) to such graph representable form. In (Bae and Tai, 2009; Ishikawa, 2003) it was observed that several surfaces can be represented by a hyper-surface in a higher dimensional domain. Hence the multi-way cut problem is equivalent to a binary cut problem in a multi-layer graph. Therefore, an extra dimension is introduced to the original graph dual

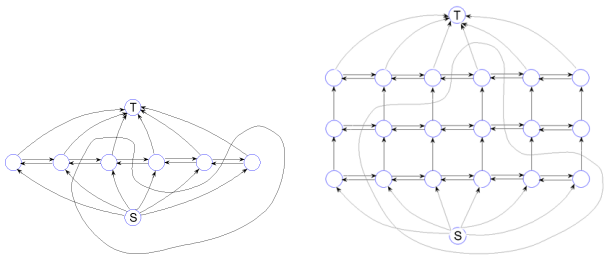

(a) two phase segmentation (b) multiphase segmentation

(c) two phase segmentation result (d) multiphase segmentation result

Fig. 4 One dimensional example to illustrate multilayer graph

to the primal mesh. This multi-layer graph idea is illustrated in Fig 4.

The multi-layer idea does not change much from image processing to surface reconstruction. As earlier, we let C_d^P denote the crust around the data points P. The domain $X \backslash C_d^P$ now contains several disconnected subdomains (instead of just two as in the last subsection). The indicator function I should be specified such that it takes different values in different subdomains

$$I(x) = \begin{cases} 0 & \text{if } x \text{ in } C_d^P \\ c_i & \text{if } x \text{ inside the } i\text{th subdomain.} \end{cases} . \tag{14}$$

Once the original graph dual to the primal mesh is constructed, it is duplicated $M-1$ times if the number of subdomains is M. More specifically, a graph is created such that $M-1$ vertices in the vertex set are associated to each tetrahedra K_i. The notation v_i^k is used for the vertex corresponding to K_i at level $k \in \{1, ..., M-1\}$. We let $c(a, b)$ denote the cost on the edge between vertex a and b. The edges constituting the data term are defined by

$$\begin{aligned} c(s, v_i^1) &= |c_1 - I(K_i)|\, \beta(K_i) \quad \text{for} \quad i = 1, ..., N, \\ c\left(v_i^k, v_i^{k+1}\right) &= |c_{k+1} - I(K_i)|\, \beta(K_i) \quad \text{for} \quad i = 1, ..., N, \\ &\quad \forall k \in \{1, ..., M-2\}, \\ c\left(v_i^{M-1}, t\right) &= |c_M - I(K_i)|\, \beta(K_i) \quad \text{for} \quad i = 1, ..., N. \end{aligned} \tag{15}$$

The weights on the horizontal edges constituting the two last terms are defined by

$$c(v_i^k, v_j^k) = (d_{ij} + \alpha) S_{ij}\,, \quad c(v_j^k, v_i^k) = (d_{ij} + \alpha) S_{ij}, \tag{16}$$

$$\forall i, j \in \{1, ..., N\}, \quad \forall k \in \{1, ..., M-1\}.$$

After finding the minimum cut $\mathcal{C}$ on this graph, the labeling function can be recovered by

$$\phi_i = \begin{cases} c_1 & \text{if} \quad (s, v_i^1) \in \mathcal{C} \\ c_{k+1} & \text{if} \quad (v_i^k, v_i^{k+1}) \in \mathcal{C}, \quad k = 1, ..., M-2 \\ c_M & \text{if} \quad (v_i^{M-1}, t) \in \mathcal{C} \end{cases} . \tag{17}$$

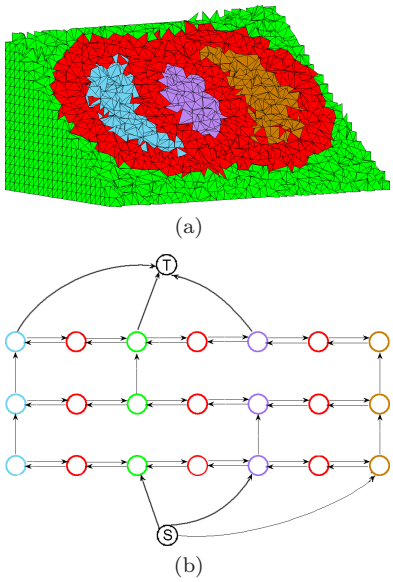

(a)

(b)

Fig. 5 Illustration on a multi-phase surface problem and the corresponding multi-layer graph.

As shown in Fig 5, the multi-layer graph idea is illustrated by two intersecting spheres. Fig 5(a) presents the cut view of the mesh, where red crust separates the domain into four regions marked with different colors. The corresponding three layer graph is shown in Fig 5(b), in which $I(K_i) = 1, 2, 3, 4$ when K_i is blue, green, purple, or brown. The nodes in the graph correspond to the tetrahedra with the same color. The weights distribution among vertical edges depend on $I(K_i)$. It is worth noticing that some vertical edges vanish as shown in (b) and the red nodes do not have vertical edges at all.

In order to determine the number of subdomains M, an intelligent method for detecting the number of subdomains based on region growing algorithms is applied after the mesh generation and crust establishment. In this procedure, the indicator function $I(K_i)$ is specified automatically. User intervention is optional, but in most cases unnecessary. As first developed in the image segmentation field, the region growing algorithm (Adams and Bischof, 1994) mainly consists of the following steps. Firstly, several initial seeds are selected. Secondly, for each seed, its neighborhood is examined to decide whether that belongs to the same partition or not. Based on this idea, a phase detection method is developed on the tetrahedral mesh, in which the neighborhood of a tetrahedron K_i are four tetrahedra sharing one face with K_i respectively. In this method, the seeds are not required to be appointed. Instead they are picked automatically during the algorithm, which is presented in Table 3 and Table 4.

Table 3 Phase detecting method based on region growing

Inputs	
1.	A mesh $\mathcal{T}_h = (P \cup Q, C), \{K_i\}_{i=1}^N \in C$
2.	Labelling values $c_i, i = 1, \ldots, M$.
Algorithm	
1.	Construct the crust K_P^M
	%% Initiate all tetrahedra
2.	For $i = 1 : N$
3.	If $K_i \in K_P^M$
4.	$I(K_i) = 0$
5.	Else
6.	$I(K_i) = -1$
7.	End If
8.	End For
	%% Region growing all tetrahedra out of crust
9.	$L = 1$
10.	For $i = 1 : N$
11.	If $I(K_i) == -1$
12.	$region\_growing(K_i, c_L)$
13.	$L = L + 1$
14.	End If
15.	End For
	%% At the end, all tetrahedra in the same partition are labeled the same value.

Table 4 Region growing function

function	$region\_growing(K, l)$
Function	
	%% $\{N_i\}_{i=1}^4$ are four neighbors of K, and l is the label value
1.	$I(K) = l$
2.	For i=1:4
3.	If $I(N_i) == -1$
4.	$region\_growing(N_i, l)$
5.	End If
6.	End For

3 Open Surface Reconstruction via Graph-cuts

The method mentioned in Section 2 can reconstruct watertight surfaces, which has an interior and exterior region in R^3. The interior region may be disconnected. In this section we discuss open surfaces, which obviously does not have a clear interior and exterior. One critical step of the previous method was the specification of the indicator function $I(x)$ as the establishment of the boundary conditions, which was completed by the phase detection method based on region growing algorithms described in Section 2. If the crust around the data set fails to separate the domain into two or more partitions as in Fig 3(b), the phase detector would label all regions out of the crust with the same indicator value. A solid and reasonable boundary condition is not available and hence the global minimum would be the trivial null surface. Therefore graph-cuts can not be conducted properly. Fig 6 illustrates this situation and the failure of our previous method by an example in two dimensions.

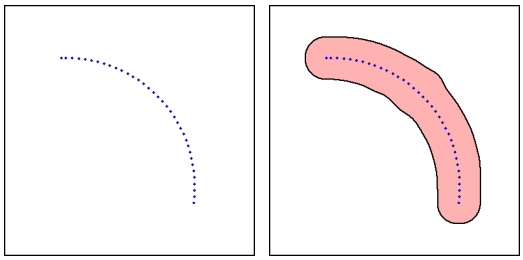

Fig. 6 Our previous method's failure on open cases where the crust fails to separate the remainder of the domain into two or more partitions.

Certain interactive specification can be used in this situation as in Fig 7(a). One spot (small region) on each side of the potential surface has been assigned with different indicator values as two 'seeds'. The graph cut result is shown in Fig 7(b). It can be noticed that the result has been artificially extended from two ends of the ground truth curve. This is inevitable since the minimal cut is required to separate the whole graph, which corresponds to the whole domain. In addition, the selection of the "seeds" spot should be rather cautious. Otherwise, improperly small "seeds" as well as a great regularization coefficient is likely to lead to a trivial result as shown in Fig 7(c), in which the cut and the corresponding surface shrink to the boundary of a "seed" spot. All these disadvantages aside, this interactive method apparently lacks generality to be applied on more complicated cases such as Fig 7(d). It is intriguing for users to select two 'seeds' in the complex spiral curve, not to mention that the graph-cuts result would be ruined by the artificially extended surface. All above considered, in this article, a more intelligent and robust reconstruction method for general surfaces, including open surfaces, watertight surfaces, and combinations of such is proposed.

As presented and illustrated above, the gap between our previous method and the new problem of open surfaces is a reasonable partitioning of the region out of the crust. The proposed method consists of an automatic partitioning procedure followed by all steps contained in Section 2. By defining a boolean operation on the vicinity of the data set, the region of interest has been trimmed in such a way that it can be separated into two or more partitions by a watertight crust. Subsequent phase detection and graph techniques can be applied on the trimmed region. Detailed description is as follows.

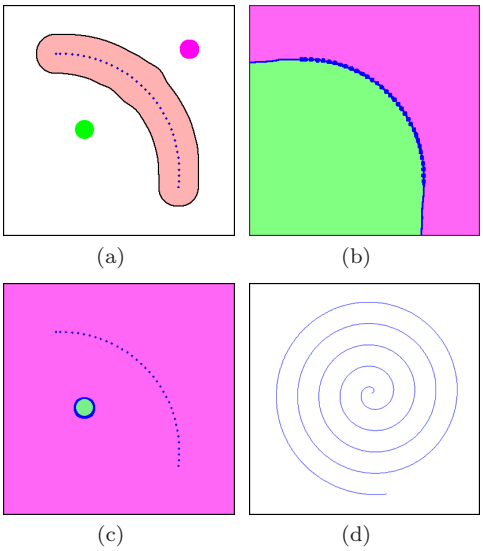

Fig. 7 An interactive method for open surface and its potential problems as well as incompetence on a complicated example.

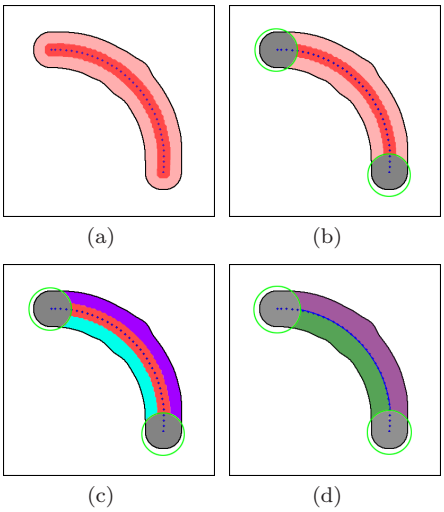

Fig. 8 Illustration on the series of crust establishments and boolean operations.

3.1 A description of the method

Given a data point set P in the domain $X \subset R^3$, which is sampled from the surface S. The distance $d(x, P)$ and the crust C_d^P is defined in the same way as in Section 2. Firstly, two crusts with different thickness parameters $d_1 < d_2$ are constructed around P: $C_{d_1}^P$ and $C_{d_2}^P$. $C_{d_2}^P$ rather than the whole domain X is the region of interest. The resulting surface is supposed to lay in $C_{d_1}^P$. These two crusts are illustrated in Fig 8(a), in which the inner crust $C_{d_1}^P$ fails to separate the region $C_{d_2}^P$ and to create a watertight environment.

Secondly the medial axis M of the boundary of $C_{d_2}^P$ is to be found. As defined in (Amenta et al, 1998), the medial axis of a manifold $\Sigma \subset R^k$ is the closure of the set of points in R^k that have at least two closest points in Σ. Under a noise-free assumption, this medial axis M itself is a good approximation to the ground truth surface S. Well approximating as it is, the medial axis is only an intermediate product of the algorithm. More steps are required to handle difficulties such as noises and non-uniformity.

Thirdly Bd, the boundary of M is found, which well approximates the boundary of the ground truth surface S. A crust around Bd is constructed: $C_{d_3}^{Bd} = \{x \in X, : d(x, Bd) \leq d_3\}$, $d_3 \geq d_2$. Subsequently those two crusts around P, i.e. $C_{d_1}^P$ and $C_{d_2}^P$, are trimmed by the crust around Bd, i.e. $C_{d_3}^{Bd}$, which can be expressed as the boolean operation: $\widetilde{C}_{d_1}^P = C_{d_1}^P - (C_{d_3}^{Bd} \cap C_{d_1}^P)$, $\widetilde{C}_{d_2}^P = C_{d_2}^P - (C_{d_3}^{Bd} \cap C_{d_2}^P)$. We can safely assert that $\widetilde{C}_{d_2}^P$ can be separated into two or more partitions by $\widetilde{C}_{d_1}^P$ given sufficient sampling and proper d_1, d_2 and d_3. This procedure is illustrated in Fig 8(b), in which Bd in two dimensions is the two ends of the curve. Two red crusts, $C_{d_1}^P$ and $C_{d_2}^P$, have been trimmed by the gray circles, i.e. $C_{d_3}^{Bd}$, and the remaining light red crust $\widetilde{C}_{d_2}^P$ is separated by the remaining dark red one $\widetilde{C}_{d_1}^P$. Hence the phase detector can label these disconnected subdomains with different indicator values and graph-cuts can be applied to the $\widetilde{C}_{d_2}^P$ as shown in Fig 8(c),(d). These two steps are same to those described in Section 2 except that the region of interest is no longer the whole domain X. As a proof of the effectiveness of the proposed method, the case in Fig 7(d) can be approached perfectly with the result shown in Fig 9.

It is worth noticing that Bd would be an empty set if the ground truth surface S is watertight. Therefore an empty crust $C_{d_3}^{Bd}$ is constructed and no boolean operation is done upon $C_{d_1}^P$ and $C_{d_2}^P$. Without this boolean operation, the method in this section has nothing different from the method described in Section 2. In other words, the method in Section 2 is a special case of the proposed method. Various types of cases, including open, watertight, and hybrid surfaces, can be approached by a single algorithm without any a priori knowledge of surface topology or beforehand hole detections.

3.2 The implementation of the method

In this subsection, we provide the discrete versions of the concepts involved in the above algorithm. This algorithm is implemented upon a tetrahedral mesh based on these discrete concepts, which is presented in detail in

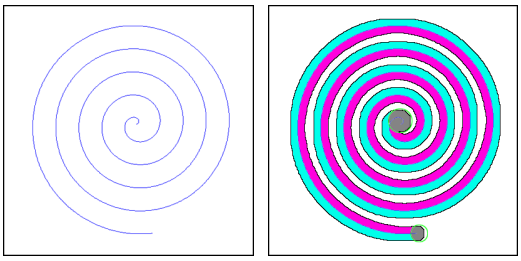

(a) (b)

Fig. 9 The case in Fig 7(d) is perfectly approached by the boolean operation method.

the Table 5. Before presenting these concepts, the establishment of the mesh framework is briefly introduced. Given a data point set P, background points Q are generated according to the local density of P. Usually, uniform or adaptive grid points are a good choice. Both P and Q are inserted into a tetrahedral mesh $\mathcal{T}_h$ in a Delaunay way. In the mesh $\mathcal{T}_h = (P \cup Q, C)$, $\{K_i\}_{i=1}^{N} \subset C$ are the tetrahedra and $\{F_i\}_{i=1}^{L} \subset C$ triangular faces.

Let the mesh and the crust be defined in the same way as in Section 2. The discrete distance between v_i and v_j is defined as $d_h(v_i, v_j) = \min_M\{M | v_j \in N_{v_i}^M\}$. Then the discrete distance between a vertex v and a vertex set V can be defined as $d_h(v, V) = \min_{x \in V} d_h(v, x)$. Further, given a surface triangulation Σ_h, the discrete medial axis can also be defined in two ways. The discrete medial axis in vertices $M_V = \{v | \exists u_1, u_2 \in \Sigma_h,$ $d_h(v, u_1) = d_h(v, u_2) = d_h(v, \Sigma_h)\}$. The discrete medial axis in triangular faces $M_F = \{F_i = \{u, v, w\} | u, v, w \in M_V\}$.

Based on these definitions in a discrete language, the proposed algorithm can be effectively implemented on a tetrahedral mesh as described in Table 5. The underlying Delaunay-based mesh makes the resulting surface more likely to be homeomorphic to the ground truth. More examples are shown in Section 5 to demonstrate the effectiveness and robustness of the proposed method.

4 Reconstruction of open surfaces based on domain decomposition

In Section 3, the open surface reconstruction method has been proposed, whose effectiveness and robustness will be shown in Section 5. The good performance on various kinds of surfaces leads to further consideration of its applications. One of the most significant applications is to reconstruct a surface based on domain decomposition. Domain decomposition has been successfully applied on computer vision field for a long time.

Table 5 Open surface reconstruction on a tetrahedral mesh

Inputs	A point set P
Algorithm	
1.	Generate background points Q according to the density of P
2.	Insert P and Q to a tetrahedral mesh $\mathcal{T}_h$ in a Delaunay way
3.	Build two crusts $K_{N_1}^P$ and $K_{N_2}^P$
4.	Find Σ, the boundary triangulation of $K_{N_2}^P$
5.	The medial axis of Σ in vertices M_V is found
6.	The medial axis of Σ in faces M_F is found
7.	The boundary of M_F is found B
8.	The vertices on the boundary B is to be found: $B_d = B \cap (P \cup Q)$
9.	Build a crust $K_{N_3}^{B_d}$ around B_d with $N_3 > N_2$
10.	Trim the two crusts around P: $\widetilde{K}_{N_1}^P = K_{N_1}^P - (K_{N_3}^{B_d} \cap K_{N_1}^P)$, $\widetilde{K}_{N_2}^P = K_{N_2}^P - (K_{N_3}^{B_d} \cap K_{N_2}^P)$
11.	Partition the region $\widetilde{K}_{N_2}^P - \widetilde{K}_{N_1}^P$ by region growing algorithms
12.	Construct a graph G dual to $\widetilde{K}_{N_2}^P$
13.	Apply graph-cuts on G and extract the surface S from the minimal cut
Outputs	The surface triangulation S

One option is to use domain decomposition idea as preconditioners to get fast solvers for some related linear problems (Kohlberger et al, 2003, 2004, 2005). Some recent analysis reveals that domain decomposition can be used as a robust alternating minimization scheme between overlapped subspaces, see (Tai and Duan, 2009; Tai and Xu, 2002). In order to use this idea for surface reconstruction, the robustness and effectiveness of such kind of divide-and-conquer algorithms will strongly depend on a good reconstruction method for general surfaces, since the surface in a subdomain may be open or have disconnected interior. Hence, based on the method proposed in Section 3, we present a reconstruction method based on domain decomposition (Tai and Duan, 2009; Tai and Xu, 2002). Since the idea of parallel reconstruction is also very attractive, the method is designed in such a way that it can easily be adapted to parallel machines.

Another motivation is the incompetence of the method proposed in Section 3 on some special cases. As is known, all 2-manifolds without boundary in R^3, i.e. watertight surfaces, are orientable. The methods dedicated to watertight surfaces don't have to face the difficulty about non-orientability. However, the 2-manifolds with boundaries, i.e. open surfaces, may be nonorientable. This nonorientable surface problem would be a great challenge for those methods based on implicit representations or graph-cuts. Therefore, the method proposed in Section 3 cannot handle nonorientable surfaces such as Mobius strip. After the trimming operation, $\widetilde{C}_{d_1}^P$ may still fail to separate $\widetilde{C}_{d_2}^P$ into two or more subdomains. A

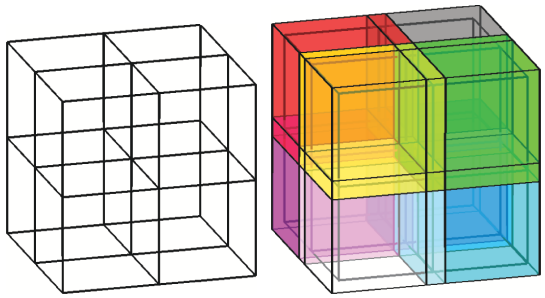

(a) (b)

Fig. 10 Nonoverlapping and overlapping decomposition schemes

surface reconstruction method based on domain decomposition would be helpful when facing this difficulty. Once the domain X has been decomposed properly, each surface piece in each subdomain is orientable, and can be approached by the method in Section 3. To the best of our knowledge, this study is the first to reconstruct non-orientable surfaces via graph-cuts.

4.1 Overlapping domain decomposition scheme

Given a domain $X \subset R^3$, a partitioning $\{X_i\}_{i=1}^N$ of X can be obtained according to a decomposition scheme. In practice, the decomposition scheme can be spatial oriented, feature oriented or data oriented. In this study, the most common spatial decomposition scheme is used. Obviously, any rectangular cuboid B can be decomposed into small tessellating rectangular cuboids $\{B_i\}_{i=1}^N$ as illustrated in Fig 10(a). In our problem, by choosing B to be a rectangular cuboid properly bounding X, i.e. $X \subset B$, $\{X_i\}_{i=1}^N$ can be obtained through $X_i = X \cap B_i$. Notice that $\cup_{i=1}^N X_i = X$, $X_i \cap X_j = \emptyset$.

Provided this partitioning is obtained and a robust reconstruction method for general surfaces such as described in Section 3 is available, the initial idea of reconstructing surfaces based on domain decomposition is simple. Decompose the input data set P into the subdomains X_i by $P_i = P \cap X_i$ and consider P_i as an independent surface reconstruction problem in X_i. A surface S_i is obtained from each P_i. The union of the reconstructed surface pieces from all subdomains $S = \cup_{i=1}^N S_i$ is taken as the final solution of reconstructing from P. This primitive divide-and-conquer method is obviously parallel friendly and easy to be implemented. However simply collecting all surface pieces from all subdomains would result in cracks as shown in Fig 11.

Usually the decomposition scheme is modified by introducing overlapping part to handle this issue. In this study, we expand cuboid cells $\{B_i\}_{i=1}^N$ to a proper extent and obtain $\{B_i'\}_{i=1}^N$ as shown in Fig 10(b). A new

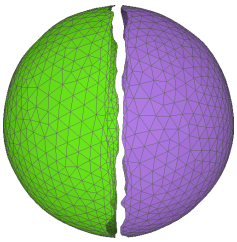

Fig. 11 Without overlapping in domain decomposition, cracks can be observed on the result surface.

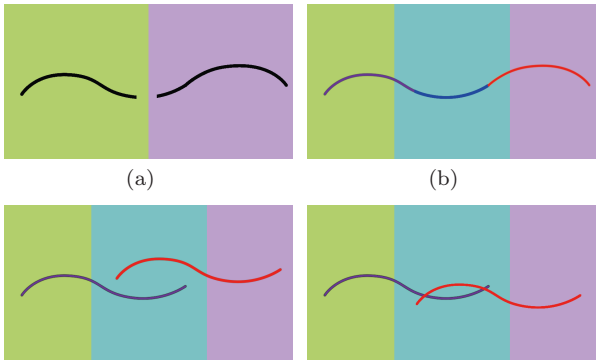

(a) (b) (c) (d)

Fig. 12 Cracks and conflicts in the overlapping part

partitioning with overlapping $\{X_i'\}$ is then obtained. Process the sub-problem of $P_i' = P \cap X_i'$ and take the union of surfaces from all subdomains $S' = \cup_{i=1}^N S_i'$ as the final result. This manner may eliminate the crack in Fig 12(a) to obtain (b). However in some cases the crack still exists in the overlapping part as shown in Fig 12(c) and sometimes worse cases are observed as the conflicting surfaces in Fig 12(d).

To tackle the issue of conflicts and cracks in overlapping part, in this study, a sequential fix-the-boundary method is proposed. As a result, some parallel potential is lost due to the increasing interaction between neighboring subdomains, which can be compensated in some degree as explained later in this section.

4.2 Fix-the-boundary reconstruction method

Without loss of generality, it is assumed that the whole domain is decomposed into only two subdomains, i.e. X_i and X_j. The partitioning with overlapping is X_i' and X_j'. The overlapping region is $X_{ij} = X_i' \cap X_j'$. Both these two partitioning systems are depicted in Fig 13(a). The sequential algorithm begins from X_i'. Once the partial data set $P_i' = P \cap X_i'$ is ready, the background points Q_i' for this subdomain are generated. Both P_i' and Q_i' are inserted into the tetrahedral mesh $\mathcal{T}_i$. Meanwhile the background points falling into the overlapping region,

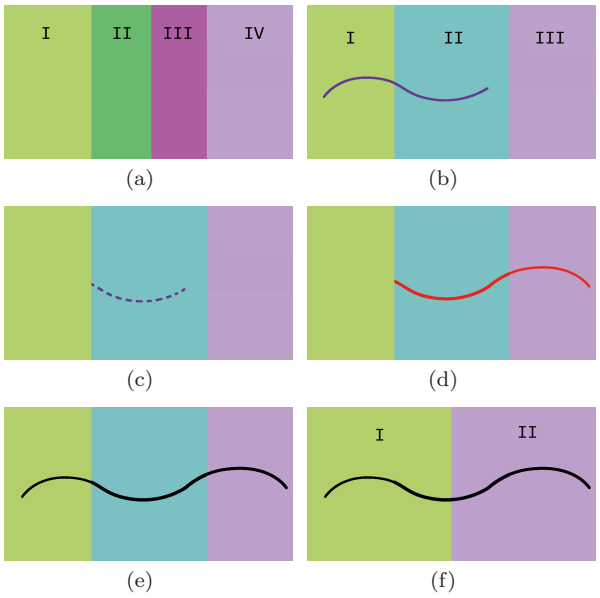

Fig. 13 A sequential fix-the-boundary method is presented to tackle cracks and conflicts. In (a), $X_i : I + II$; $X_j : III + IV$. $X_i^{'} : I + II + III$; $X_j^{'} : II + III + IV$. In (b)-(e), $X_i^{'} : I + II$; $X_j^{'} : II + III$; $X_{ij} : II$. In (f), $X_i : I$; $X_j : II$.

i.e. $Q_i^{'} \cap X_{ij}$ are stored. The graph-based method is applied and the reconstruction result $S_i^{'}$ is obtained as in Fig 13(b). The reconstructed surface falling into the overlapping region, i.e. $S_i^{'} \cap X_{ij}$ is also stored for further use as in Fig 13(c).

When the second subdomain $X_j^{'}$ is processed, one measure is taken upon the background points. After the background points $Q_j^{'}$ for $X_j^{'}$ are generated, the background points falling into the overlapping region are replaced by those background points stored in the $X_i^{'}$ stage: $Q_j^{'} = (Q_j^{'} - X_{ij}) \cup (Q_i^{'} \cap X_{ij})$. This operation ensures that the two subdomains contain the same background points in the overlapping region, i.e. $Q_i^{'} \cap X_{ij} = Q_j^{'} \cap X_{ij}$. The same data points and background points add up to an identical mesh point set in the overlapping region. Under the assumption of general positions, the Delaunay triangulation of a point set is unique. Combined with the local property of Delaunay triangulations, it is safe to assert that the meshes in the overlapping region from two subdomains are identical, i.e. $\mathcal{T}_i \cap X_{ij} = \mathcal{T}_j \cap X_{ij}$, which guarantees that $S_i^{'} \cap X_{ij} \subset \mathcal{T}_j \cap X_{ij}$.

Following the routine of the graph-based method, a graph is constructed dual to the mesh $\mathcal{T}_j$. Then we increase the weights of those edges corresponding to the stored faces $S_i^{'} \cap X_{ij}$, to a relatively large value. Through this adjustment, the surface $S_j^{'}$ reconstructed in $X_j^{'}$ is forced to coincide with $S_i^{'}$ in the overlapping region, i.e. $S_i^{'} \cap X_{ij} = S_j^{'} \cap X_{ij}$ as in Fig 13(d). The surface in the overlapping region X_{ij} serves as the boundary of both $S_i^{'}$ and $S_j^{'}$. In the $X_i^{'}$ stage, the choice of the boundary of $S_i^{'}$ is relaxed. In the $X_j^{'}$ stage, the boundary of $S_j^{'}$, i.e. $S_j^{'} \cap X_{ij}$, will be fixed through the adjustment on the edge weight assignment. Hence conflicts and cracks can be avoided as in Fig 13(e). We refer to this adjustment of the edge weight as "fix the surface in X_{ij}" for short.

Furthermore, some measures are taken to eliminate the redundant output of surface. Notice the curve in the overlapping region in Fig 13(e) has been outputted twice in two stages. This redundant output is harmless and can be eliminated by a trimming operation. After the surface piece $S_i^{'}$ in each subdomain is obtained, the non-overlapping decomposition X_i is used to trim the surface piece, i.e. $S_i = S_i^{'} \cap X_i$. The union of all trimmed surface pieces $S = \cup_{i=1}^{N} S_i$ is the final result, which is free of redundant output, cracks or conflicts as in Fig 13(f). The whole divide-and-conquer algorithm is given in Table 6.

4.3 Parallel efficiency regained

As mentioned, some parallel potential is lost due to the interaction between subdomains in this method. Two neighboring subdomains cannot be processed simultaneously. As in the example of Fig 13, the subdomain $X_j^{'}$ cannot be processed until $S_i^{'} \cap X_{ij}$ is obtained. To adapt this method to parallel machines, it would be helpful to color all subdomains at the beginning so that no neighboring subdomains have the same color. Then the group of subdomains sharing the same color can be processed simultaneously because of the independence between any two of them. This coloring preprocessing turns the sequential algorithm in Table 6 to a parallel algorithm. However the coloring strategy and the number of colors required determine the parallel efficiency.

In two dimensional problems such as image segmentation (Hodneland et al, 2009), the well known four-color theorem can limit the number of the colors required within four. Unfortunately, there is no such theoretic bound of the number of colors required in three dimensions. However, for some special cases, we still can figure out the number of colors required. For the rectangular cuboids decomposition scheme described above and the underlying 26-neighborhood system, it can easily be shown that only eight colors are required for a neighbor-different coloring. An example of $5 \times 5 \times 5$ decomposed cube's 8 coloring scheme is shown in Fig 14. The parallel efficiency of these decomposition cases is still high even with the dependence between subdomains.

Table 6 Algorithm of surface reconstruction based on domain decomposition

Inputs	
1.	A point set P
2.	Partition of X, $\{X_i\}_{i=1}^N$
3.	Partition of X with overlapping, $\{X_i^{'}\}_{i=1}^N$
4.	$Neigh_i[N_i]$, $i = 1, \cdots, N$, N_i is the number of neighbors of X_i, and the array $Neigh_i$ stores N_i neighbors.
Algorithm	
1	Initialize a flag matrix $\{F_{ij}\} = 0$
2	Allocate storage for Q_{ij} background points in X_{ij}
3	Allocate storage for S_{ij} the surface in X_{ij}
4	For $i = 1 : N$
5	$P_i^{'} = P \cap X_i^{'}$
6	Generate $Q_i^{'}$ according to $P_i^{'}$
7	For $k = 1 : N_i$
8	$j = Neigh_i[k]$
9	if $F_{ij} == 1$
10	$Q_i^{'} = (Q_i^{'} - X_{ij}) \cup Q_{ij}$
11	else
12	$Q_{ij} = Q_{ji} = Q_i^{'} \cap X_{ij}$
13	End if
14	End For
15	Insert $P_i^{'}$ and $Q_i^{'}$ to generate the mesh $\mathcal{T}_i$
16	For $k = 1 : N_i$
17	$j = Neigh_i[k]$
18	if $F_{ij} == 1$
19	Fix all S_{ij} in X_{ij}
20	$F_{ij} = F_{ji} = 1$
21	End if
22	End For
23	Apply graph-based method and obtain $S_i^{'}$
24	Trim the surface piece $S_i = S_i^{'} \cap X_i$
25	End For
Outputs	The surface triangulation $S = \bigcup_{i=1}^{N} S_i$

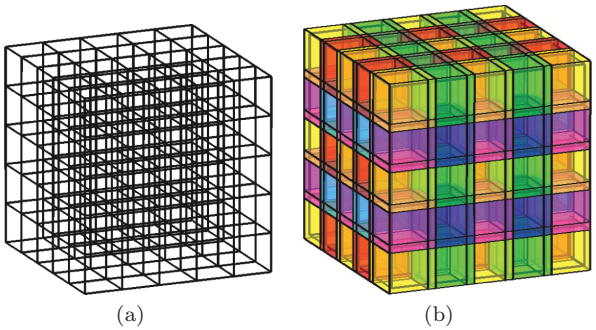

Fig. 14 Eight Coloring Scheme

In this section, a new reconstruction method based on domain decomposition was proposed. Interaction between subdomains was introduced to eliminate possible cracks and conflicts. Though this interaction between subdomains requires a sequential algorithm, a proper decomposition manner as well as a coloring preprocessing allows for parallel algorithms. Some examples approached by this decomposition based method are included in Section 5 to show its robustness and effectiveness.

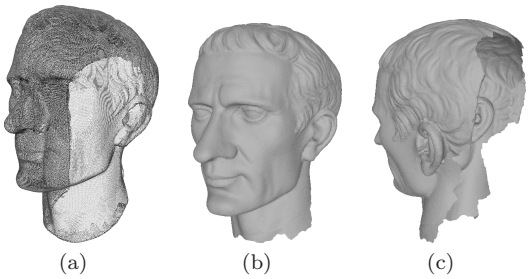

Fig. 15 Julius Caesar

5 Examples

In this section, various examples are presented to demonstrate the efficiency and robustness of our method as well as the quality and faithfulness of reconstructed surfaces. All experiments had been conducted on a desktop PC with Intel Pentium 4 CPU of 3.2GHz. Most models were obtained from Stanford 3D Scanning Repository, Large Geometric Models Archive of Georgia Institute of Technology and Digital Shape Workbench Project while the others were synthesized by ourselves. All surfaces are rendered by MeshLab. Only points locations were utilized in the algorithm. Based on the properties and purposes of theirs, these examples can be categorized into four groups: simple open surfaces, complicated (general) surfaces, watertight surface approached by domain decomposition, and non-orientable surfaces approached by domain decomposition.

5.1 Simple open surfaces

Simple open surfaces generally refer to manifolds with boundaries. As the initial motivation of this study, several examples of the simple open surfaces are demonstrated in Fig 15, 16, and 17 including the data point sets and the reconstructed surfaces. Two human faces, one representative category of open surfaces, are faithfully reconstructed. The front views show the well-preserved features and the back or bottom view shows the boundaries of reconstructed surfaces. The other example, a hand is presented as well. All these three examples can be seen as the application on incomplete data. After all, it is hardly possible to obtain watertight models of human body parts by a 3D laser scanner.

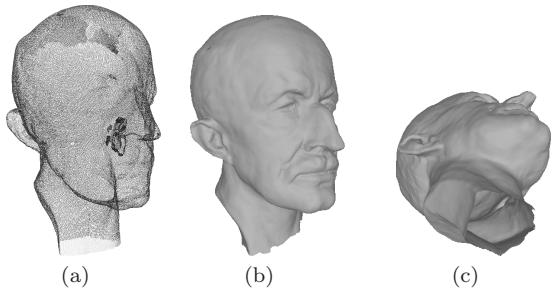

Fig. 16 Max Planck

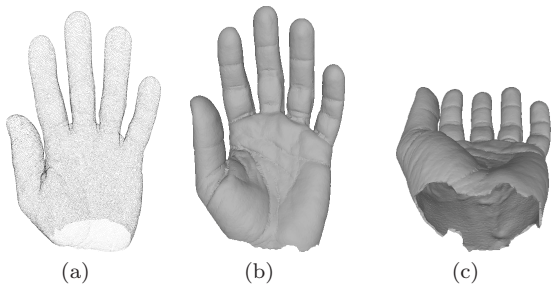

Fig. 17 Oliever's hand

5.2 Complicated (General) surfaces

Since simple open surface cases can be approached perfectly, the proposed method is challenged by some more complicated examples: multi-phase open surfaces, hybrids of open and watertight surfaces, and open surfaces with noises. To sum up, this subsection presents surface examples which are more general and occur ubiquitously in daily life.

Multi-phase open surfaces do not have to separate the domain into more than two regions. Multi-phase means the trimmed crust $\widetilde{C}^P_{d_2}$ is partitioned by $\widetilde{C}^P_{d_1}$ into more than two regions. These cases may involve intersections or not. Multi-phase cases without intersections, i.e. disconnected surface patches, are still 2-manifolds with boundaries and apparently no challenge to the proposed method. Furthermore, the approaching to an example of two intersecting semi-spheres, which is no longer 2-manifold, is shown in Fig 18, from which we can see that all features of the intersecting parts are reconstructed faithfully.

The above example can be seen as a union of two 2-manifolds, both of which have boundaries. Next presented is a union of two 2-manifolds, one of which has boundaries while the other has not, i.e. a union of a water tight surface and an open one. The reconstruction result of a rectangle intersecting a sphere is shown in Fig 19, from which we can see that both the sphere and the rectangle have been reconstructed faithfully. From

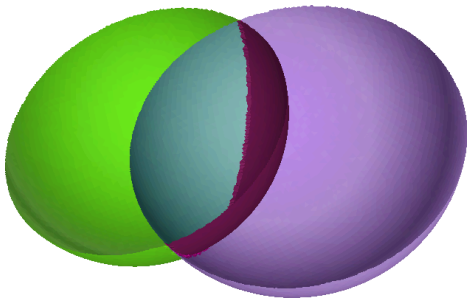

Fig. 18 A multi-phase open surface example: two intersecting semi-spheres.

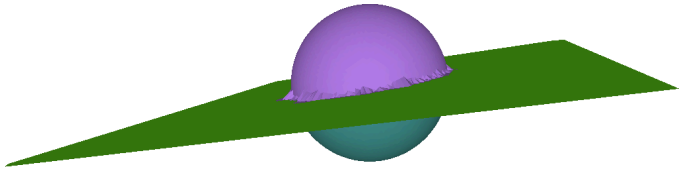

Fig. 19 A hybrid of a watertight surface and an open one: a rectangle intersecting a sphere.

a technical point of view, this example has nothing special compared to the one in Fig 18. It becomes, however, more meaningful after post-processing. The watertight sphere surface can be thought of as the boundary of a 3-manifold ball. Once the domain bounded by the sphere is volumetrically meshed, the union of the 3-manifold and the 2-manifold can be represented discretely by a triangular and tetrahedral mixed mesh. This issue ubiquitously occurs in animations, medical applications, and CAD industries.

The last example in this subsection is an open surface with noise. The noises in real world may be introduced during the data acquisition procedure. In this study, the noise is added artificially. The data set in blue as well as the noise in red is shown in Fig 20(a). This distinguishing coloring scheme is only for clear demonstration and the algorithm treats data and noise in a same manner. Fig 20(b) and (c) show results with regularization coefficient $\alpha = 0$ and 0.001 respectively. The noise removal result with $\alpha = 0.001$ is zoomed and shown in Fig 20(d).

5.3 Watertight surfaces approached by domain decomposition

Surface reconstruction based on domain decomposition is an important application of the open surface reconstruction method. In this subsection, some watertight cases, which had been perfectly approached by previous graph-cuts methods, are used to test the effectiveness

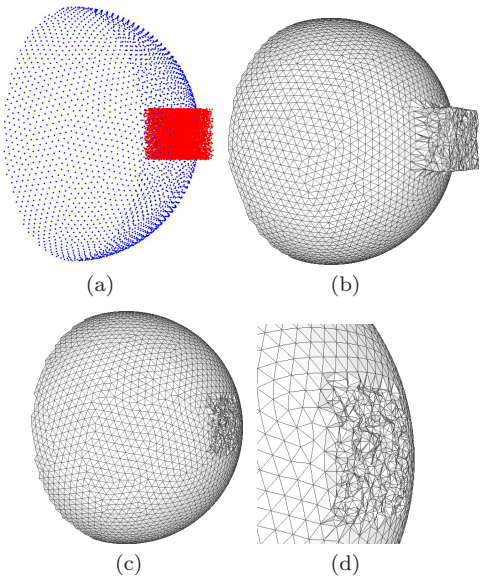

Fig. 20 The noisy case of a semi-sphere

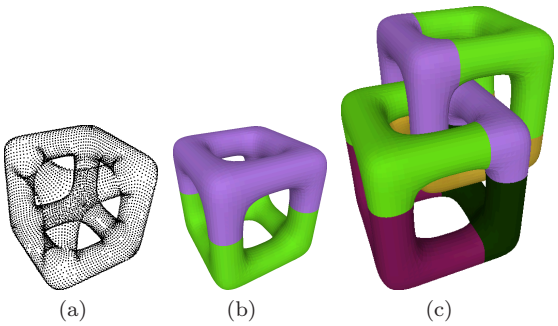

Fig. 21 Perforated cubes approached by domain decomposition

of the decomposition based reconstruction method, especially the overlapping and interface part.

Fig 21 shows that two cube-based objects are reconstructed in a domain decomposition way. The perforated cube in Fig 21(b) is reconstructed in two subdomains as different colors indicate. Similarly, two tangling perforated cubes in Fig 21(c) has been approached in eight subdomains, each of which contains multiple disconnected surface patches. These are same to the results obtained by previous methods.

Next three classic examples, armadillo, horse, and dragon, are shown in Fig 22. The colorfulness of armadillo is used to illustrate the relationship between the choice of thickness parameters, d_1 and d_2, and the multiphase issue. Once we increase the difference between d_1 and d_2, the colorfulness disappears gradually as the phase number decreases, which is shown in the horse and dragon examples.

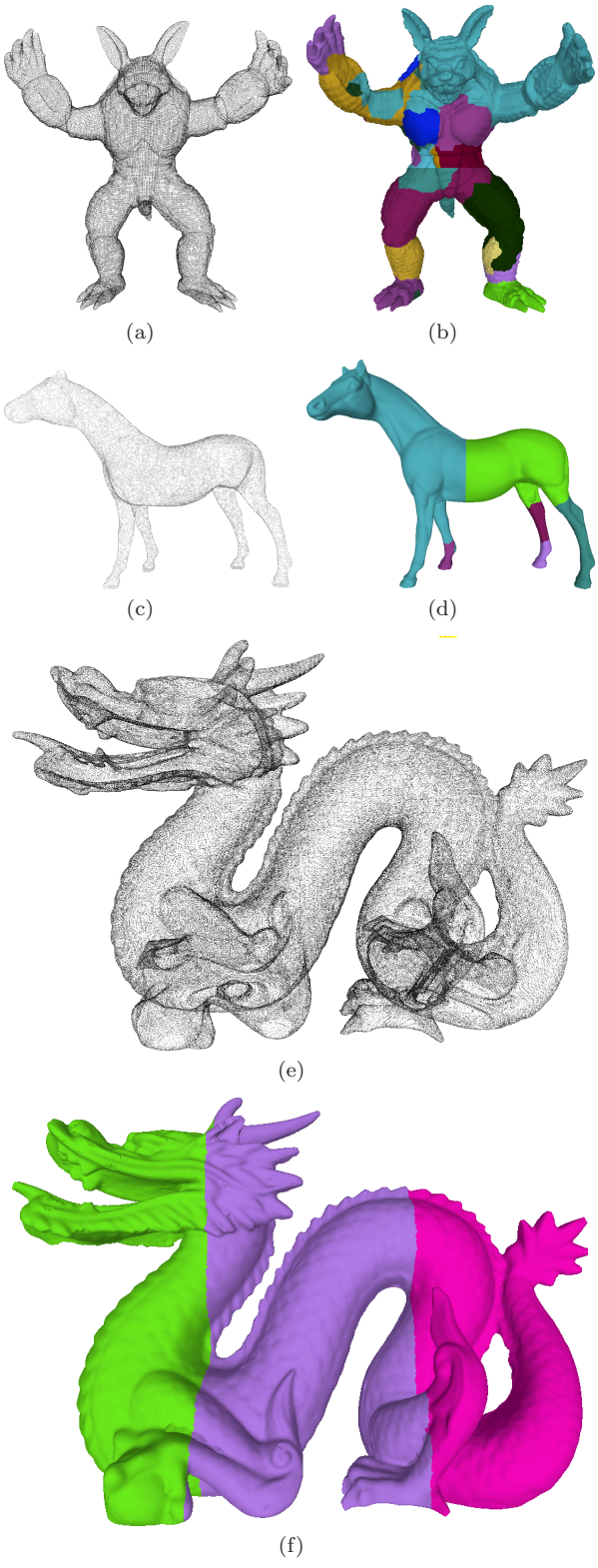

Fig. 22 Three classical examples approached by domain decomposition

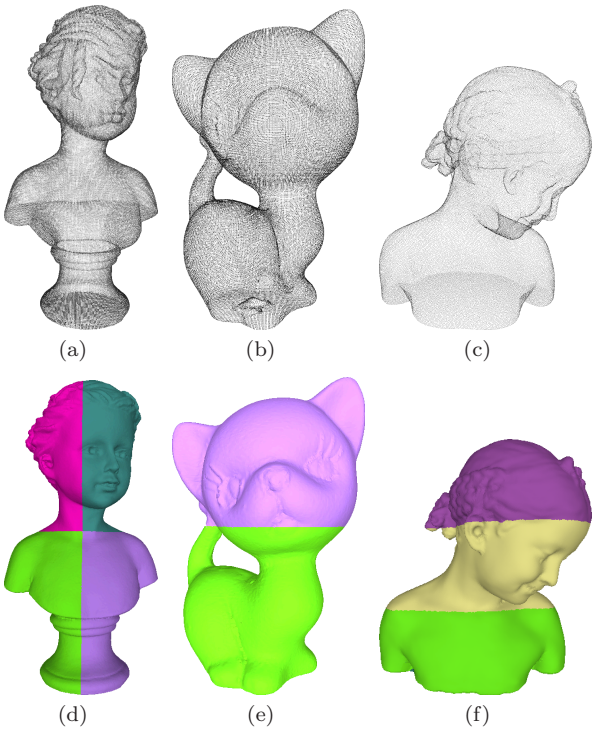

Fig. 23 Three statuettes approached in different decomposition schemes

At last of this subsection, three statuettes are shown in Fig 23. From left to right, the statuettes are reconstructed in four, two and three subdomains respectively. Through this subsection, the absence of undesirable conflicts and cracks as Fig 12(c) and (d) proves the effectiveness of our method.

5.4 Nonorientable Surfaces

As mentioned, when the research area is extended to the open surfaces, i.e. 2-manifolds with boundaries, the nonorientable issue becomes a problem for all graph-based methods. In this subsection, Mobius strip, one motivation of this decomposition based method, is approached perfectly with the result shown in Fig 24. Another famous nonorientable surface, Klein bottle, is also presented in Fig 25.

Table 7 gives the sizes of the data sets of several open surface examples and corresponding CPU time counted in seconds. The first column gives the examples' names. The second column contains the numbers of data points P. The third column is the mesh generation time, the fourth the graph construction time, and

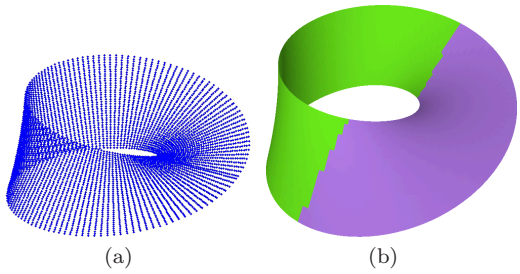

Fig. 24 Mobius strip approached by domain decomposition method.

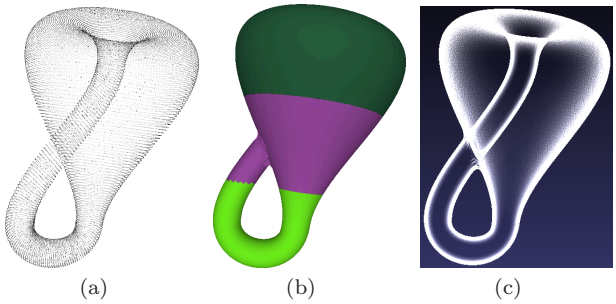

Fig. 25 Klein bottle approached by domain decomposition method.

Table 7 Statistics of open surface examples

Example	Data Set	Mesh Generation Time	Graph Built Time	Graph Cut Time
Caesar	387900	248.4952	7.48386	22.3256
Planck	199169	96.7383	5.2332	9.8995
Hand	53054	41.37467	1.16082	8.49171

the fifth the graph cut time. In Table 8 included are sizes and time of the domain decomposition examples. Each block contains the statistics of every subdomain as well as those in total.

6 Conclusion

In this article, a variational reconstruction method for open surface is proposed based on Delaunay triangulation and graph-cuts. In the proposed method, the graph is constructed dual to the mesh in a restricted region obtained after crust establishments and boolean operations, by which the open surface problem in the whole domain has been translated to a watertight surface problem in a restricted region. The phase detection based on region growing algorithms hence can be applied and so can the graph techniques.

Furthermore, a surface reconstruction method based on domain decomposition is presented as an important application of open surface reconstruction. One motiva-

Table 8 Statistics of domain decomposition examples

Example	Data Set	Mesh Generation Time	Graph Built Time	Graph Cut Time
Armadillo Total	172974	191.58093	4.74328	3.936398
Subdomain 1	76525	73.61781	1.78773	3.06553
Subdomain 2	119073	117.96312	2.95555	0.870868
Horse Total	494195	843.2701	16.12855	12.67107
Subdomain 1	300357	315.7326	7.78682	5.00724
Subdomain 2	299595	527.5375	8.34173	7.66383
Dragon Total	437645	605.4991	15.40466	2.239658
Subdomain 1	190871	259.2044	4.87826	0.151977
Subdomain 2	265931	346.2947	6.66699	1.9627
Subdomain 3	155873	194.8477	3.85941	0.124981

tion is parallel surface reconstruction. However, overlapping regions are introduced and the independence between subdomains are sacrificed to eliminate the conflicts and cracks. This loss of parallel potential may be largely compensated if we adopt proper decomposition scheme. By the decomposition scheme in this paper, if the numbers of processing units and subdomains are both larger than eight, the parallel efficiency is as high as a subdomain-independent algorithm. Implementation of this domain decomposition method and investigation of its efficiency is one of our future research interests.

Acknowledgements This research is sponsored by Sinapore MOE ARC 29/07 T207B2202, MOE RG 59/08 M52110092, and NRF 2007IDM-IDM 002-010.

References

Adams R, Bischof L (1994) Seeded region growing. IEEE Transactions on Pattern Analysis and Machine Intelligence 16(6):641–647

Adamy U, Giesen J, John M (2000) New techniques for topologically correct surface reconstruction. In: Proceedings of the conference on Visualization'00, IEEE Computer Society Press Los Alamitos, CA, USA, pp 373–380

Alexa M, Behr J, Cohen-Or D, Fleishman S, Levin D, Silva C (2001) Point set surfaces. In: IEEE Visualization, vol 1, pp 21–28

Amenta N, Bern M, Kamvysselis M (1998) A new Voronoi-based surface reconstruction algorithm. In: Proceedings of the 25th annual conference on Computer graphics and interactive techniques, ACM New York, NY, USA, pp 415–421

Amenta N, Choi S, Dey T, Leekha N (2000) A simple algorithm for homeomorphic surface reconstruction. In: Proceedings of the sixteenth annual symposium on Computational geometry, ACM New York, NY, USA, pp 213–222

Bae E, Tai XC (2009) Graph cut optimization for the piecewise constant level set method applied to multiphase image segmentation. In: Tai XC, Morken K, Lysaker M, Lie KA (eds) SSVM, Springer, Lecture Notes in Computer Science, vol 5567, pp 1–13

Bertalmío M, Sapiro G, Randall G (1999) Region tracking on surfaces deforming via level-sets methods. Lecture notes in computer science pp 330–338

Boissonnat J, Cazals F (2000) Smooth surface reconstruction via natural neighbour interpolation of distance functions. In: Proceedings of the sixteenth annual symposium on Computational geometry, ACM New York, NY, USA, pp 223–232

Boykov Y, Kolmogorov V (2004) An experimental comparison of min-cut/max-flow algorithms for energy minimization in vision. IEEE Transactions on Pattern Analysis and Machine Intelligence pp 1124–1137

Burchard P, Cheng L, Merriman B, Osher S (2001) Motion of curves in three spatial dimensions using a level set approach. Journal of Computational Physics 170(2):720–741

Caselles V, Kimmel R, Sapiro G (1997a) Geodesic active contours. International journal of computer vision 22(1):61–79

Caselles V, Kimmel R, Sapiro G, Sbert C (1997b) Minimal surfaces based object segmentation. IEEE Transactions on Pattern Analysis and Machine Intelligence 19(4):394–398

Cheng L, Burchard P, Merriman B, Osher S (2002) Motion of curves constrained on surfaces using a level-set approach. Journal of Computational Physics 175(2):604–644

Curless B, Levoy M (1996) A volumetric method for building complex models from range images", SIGGRAPH96. In: Computer Graphics Proceedings

Dey TK, Goswami S (2003) Tight cocone: a water-tight surface reconstructor. In: SM '03: Proceedings of the eighth ACM symposium on Solid modeling and applications, pp 127–134

Edelsbrunner H, Mucke E (1992) Three-dimensional alpha shapes. In: Proceedings of the 1992 workshop on Volume visualization, ACM New York, NY, USA, pp 75–82

Faugeras O, Gomes J (2000) Dynamic shapes of arbitrary dimension: the vector distance functions. In: Proceedings of the Ninth IMA Conference on Mathematics of Surfaces. The Mathematics of Surfaces IX, Springer, Citeseer

Franchini E, Morigi S, Sgallari F (2010a) Implicit shape reconstruction of unorganized points using PDE-based deformable 3D manifolds. Numerical Mathematics: Theory, Methods and Applications

Franchini E, Morigi S, Sgallari F (2010b) Segmentation of 3D Tubular Structures by a PDE-Based Anisotropic Diffusion Model. Mathematical Methods for Curves and Surfaces pp 224–241

George P, Borouchaki H (1998) Delaunay triangulation and meshing: application to finite elements. Kogan Page

Hodneland E, Tai X, Gerdes H (2009) Four-Color Theorem and Level Set Methods for Watershed Segmentation. International Journal of Computer Vision 82(3):264–283

Hoppe H, DeRose T, Duchamp T, McDonald J, Stuetzle W (1992) Surface reconstruction from unorganized points. In: SIGGRAPH '92: Proceedings of the 19th annual conference on Computer graphics and interactive techniques, pp 71–78

Hornung A, Kobbelt L (2006a) Hierarchical volumetric multi-view stereo reconstruction of manifold surfaces based on dual graph embedding. In: 2006 IEEE Computer Society Conference on Computer Vision and Pattern Recognition, vol 1

Hornung A, Kobbelt L (2006b) Robust reconstruction of watertight 3d models from non-uniformly sampled point clouds without normal information. In: Geometry Processing 2006: Fourth Eurographics Symposium on Geometry Processing, Cagliari, Sardinia, Italy, June 26-28, 2006, Eurographics, p 41

Ishikawa H (2003) Exact optimization for markov random fields with convex priors. IEEE Transactions on Pattern Analysis and Machine Intelligence 25(10):1333–1336

Kohlberger T, Schnörr C, Bruhn A, Weickert J (2003) Domain decomposition for parallel variational optical flow computation. Pattern Recognition pp 196–203

Kohlberger T, Schnörr C, Bruhn A, Weickert J (2004) Parallel variational motion estimation by domain decomposition and cluster computing. Computer Vision-ECCV 2004 pp 205–216

Kohlberger T, Schnörr C, Bruhn A, Weickert J (2005) Domain Decomposition for Nonlinear Problems: A Control-Theoretic Approach. Technical Report, Computer Science Series

Kolmogorov V, Zabin R (2004) What energy functions can be minimized via graph cuts? IEEE Transactions on Pattern Analysis and Machine Intelligence 26(2):147–159

Lempitsky VS, Boykov Y (2007) Global optimization for shape fitting. In: CVPR, IEEE Computer Society

Lie J, Lysaker M, Tai X (2006) A variant of the level set method and applications to image segmentation. Mathematics of computation 75(255):1155–1174

Ohtake Y, Belyaev A, Alexa M, Turk G, Seidel H (2005) Multi-level partition of unity implicits. In: International Conference on Computer Graphics and Interactive Techniques, ACM New York, NY, USA

Osher S, Fedkiw R (2002) Level set methods and dynamic implicit surfaces. Springer Verlag

Paris S, Sillion F, Quan L (2006) A surface reconstruction method using global graph cut optimization. International Journal of Computer Vision 66(2):141–161

Smereka P (2000) Spiral crystal growth. Physica D: Nonlinear Phenomena 138(3-4):282–301

Solem J, Heyden A (2004) Reconstructing open surfaces from unorganized data points. In: IEEE Computer Society Conference on Computer Vision and Pattern Recognition, IEEE Computer Society; 1999, vol 2

Solem J, Heyden A (2006) Reconstructing open surfaces from image data. International Journal of Computer Vision 69(3):267–275

Solem J, Kahl F (2004) Surface reconstruction from the projection of points, curves and contours. In: 2nd Int. Symposium on 3D Data Processing, Visualization and Transmission, Thessaloniki, Greece

Solem J, Kahl F (2005) Surface reconstruction using learned shape models. Advances in Neural Information Processing Systems 17:1

Solem J, Overgaard N (2005) A geometric formulation of gradient descent for variational problems with moving surfaces. In: International Conference on Scale Space and PDE Methods in Computer Vision, Springer, pp 419–430

Tai X, Duan Y (2009) Domain decomposition methods with Graph cuts algotithms for image segmentation. UCLA CAM Report pp 9–54

Tai X, Xu J (2002) Global and uniform convergence of subspace correction methods for some convex optimization problems. Mathematics of Computation 71(237):105–124

Wan M, Wang Y, Wang D (to appear) Variational Surface Reconstruction Based on Delaunay Triangulation and Graph Cut. Int J Numer Meth Eng

Ye J, Bresson X, Goldstein T, Osher S (2010) A Fast Variational Method for Surface Reconstruction from Sets of Scattered Points. UCLA CAM Report

Zhao H, Osher S, Fedkiw R (2001) Fast surface reconstruction using the level set method. In: Proceedings of the IEEE Workshop on Variational and Level Set Methods (VLSM'01), IEEE Computer Society Washington, DC, USA, p 194

Zhao M (2000) Implicit and nonparametric shape reconstruction from unorganized data using a variational level set method. Computer Vision and Image Understanding 80(3)